

Impact-aware humanoid robot motion generation with a quadratic optimization controller

Yuquan Wang¹, Arnaud Tanguy, Pierre Gergondet and Abderrahmane Kheddar

Abstract—Impact-aware tasks (i.e. on purpose impacts) are not handled in multi-objective whole-body controllers of humanoid robots. This leads to the fact that a humanoid robot typically operates at near-zero velocity to interact with the external environment. We explicitly investigate the propagation of the impact-induced velocity and torque jumps along the structure linkage and propose a set of constraints that always satisfy the hardware limits, sustain already established contacts, and the stability measure, i.e. the zero moment point condition. Without assumptions on the impact location or timing, our proposed controller enables humanoid robots to generate non-zero contact velocity without breaking the established contacts or falling. The novelty of our approach lies in building on existing continuous dynamics whole body multi-objective controller without the need of reset-maps or hybrid control.

I. INTRODUCTION

Advanced humanoids capabilities such as walking and manipulation improved substantially in recent years. Yet, when it comes into general-purpose loco-manipulation, humanoid robots fear impacts similarly to most existing robots. Dealing with task-aware impacts –e.g. on purpose impact tasks such as pushing (see Fig. 1) and even hammering or landing at jumps... or non-desired impacts –e.g. those consequent to falls, requires capabilities in both the hardware design and the controller aspects.

Impacts last a very short of time [1] (in theory, it is instantaneous), in which a considerable amount of energy is propagated through the structure and linkage of the humanoid robot and could potentially result in (i) hardware damage, and (ii) a jump in some or all unilateral contacts that existed before impact. A large part of handling impact must be tackled from a hardware perspective that we do not address in this paper. We rather assume that we possess knowledge on tolerable impact bounds, that the linkage mechanics, actuators, and electronics can absorb without damage. Indeed, no controller can deal with any strategy at the very impact-instant: the energy shall simply be absorbed by the hardware. However, a controller can be designed to act before and after the impact, most robustly and stably.

It is not easy to design an impact-aware whole body controller that can achieve on-purpose impact tasks due to the following facts:

- (1) impacts induce jumps in part of the robot state: that is, abrupt changes of the joint velocities, torques, and –in the case of humanoids, unilaterally established contact forces;
- (2) Due to the jumps, the robot dynamics (equations of

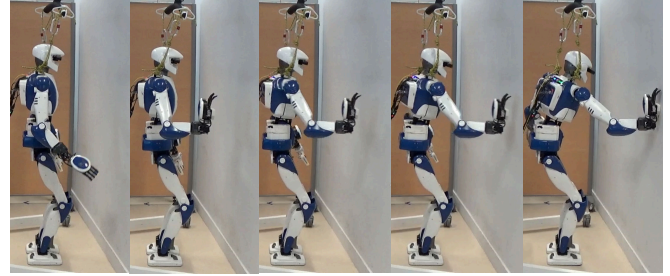


Fig. 1: Snapshots of the HRP-4 robot pushing a concrete wall. The contact velocity is 0.35 m/s at the impact time which is determined from force sensor readings.

motions) are different and a reset map is needed;

- (3) the difficulty (if not the impossibility) to know precisely some pertinent parameters, such as the environment stiffness, the coefficient of restitution, the impact localization on the robot (and the environment), the contact normal, and the exact impact time;

These parameters are pertinent to model impact dynamics and their uncertainty might cause undesired post-impact status, e.g. rebound or sliding. Therefore a common practice is to set and release a contact at near-zero velocity to ensure a smooth contact transition without invoking impacts.

We propose to overcome these limitations by integrating the impact dynamics model into our whole-body multi-objective continuous dynamics controller (and not specifically design a dedicated controller to handle task-aware impact). This choice is very important and constitutes the main novelty and the most appealing aspect of our approach w.r.t. e.g. existing task-specific controllers, reset map controllers or hybrid controllers, etc. The main idea is to guarantee, through considering upper-bounds, the worst-case impact situations such that the robot motion is robust to an impact whose exact timing, location, and other pertinent parameters that might be not known exactly.

Our whole-body robot controller is formulated as quadratic programming in the task space [2]. We have demonstrated our controller with very complex multi-objective dynamic operations and embed already visual servoing, force control, set-point and trajectory tracking tasks under various types of constraints such as joint limits, collision avoidance, etc. Our main goal is to extend this controller with multi-purpose impact-aware tasks with minimal structural changes and if possible, no particular switching or *if-then-elses*, i.e. only by designing additional impact-aware constraints and tasks that can be added or removed at will and on-purpose. We stress

¹ CNRS-University of Montpellier, LIRMM, Interactive Digital Humans group, Montpellier, France. Email: {yuquan.wang, arnaud.tanguy, pierre.gergondet, kheddar}@lirimm.fr

on the importance of this choice because it allows having an enhanced integrated multi-purpose control framework.

In our previous work [3], we show that for a fixed-based robot, hardware limitations in terms of max allowable impact can be easily integrated as additional constraints in our controller. Yet, such constraints do not prohibit jumps in the joint velocities and torques that could make the controller computation fails or diverge in a closed-loop scheme. This is because, right after the impact, the QP solver might start from an unfeasible constraints set. These facts are obviously found in humanoid robots too. In humanoids, we also have unilateral contacts setting and a floating (under-actuated) base: not only the joint velocities and torques undergo an abrupt more or less substantial change, but so does each contact forces. By applying impact dynamics analysis to the operational space equations of motion, one can model the propagation of the state jumps between the end-effectors, see Sec. IV.

Moreover, the dynamic balance of humanoid robots – eventually through the Zero Moment Point (ZMP), under impacts has been investigated for planning purposes in specific tasks [4], [5]. A multi-objective controller that fulfills the dynamic balance constraint under impacts is, to our best knowledge, missing, see Sec. II. Indeed, sustaining at best prior contacts and balance during impacts is a fundamental issue that is not yet explicitly addressed in any existing QP controller frameworks. We highlight this gap in Sec. III based on the analysis performed on a state-of-the-art QP controller. We analytically derive inequality constraints to generate feasible robot motion such that the impact-induced state jumps will not break the contact and balance conditions regardless of the impulsive forces.

We assess our impact-aware multi-objective QP controller using an HRP-4 humanoid robot that impacts a fixed concrete wall without knowing exactly its location in Sec. V. The impact-awareness enables a humanoid robot to apply impacts without stopping or reducing speed.

II. RELATED WORK

Impact duration analysis in [4], [6] revealed that even for low-velocity, the duration of an impact is typical of milliseconds order or less. In such a short period it is difficult to devise an efficient controller that prevents hardware to be hindered to some extent. For instance, even if a variable stiffness actuator lower damage risks at impacts, it needs more than 10 ms to generate the joint torque that can counterbalance the impulsive torques [7]. Therefore, our controller doesn't consider and is independent of impact timing.

The discrete impact dynamics model has been introduced into robotics since late 1980 [1]. Yet, more refined physics laws for multiple contacts and impacts are not known for inelastic impacts until around 2010 [8], [9]. Recently a flying object batting example is developed in [10], where a closed-form 2D impact dynamics model is used to generate desired impulsive forces. However in the 3D cases, the closed-form solution is only available if we can control the

initial sliding direction to the invariant subset [11]. Thus we restrict ourselves to the impact models based on algebraic equations [1] that have been successfully applied in multiple scenarios [4], [5], [12]. To our best knowledge, on-purpose impact tasks are studied only in very few work e.g. in [5] for specific tasks. However, their controller doesn't account for uncertainties in most impact parameters, it is based on a non-linear optimization for planning, and doesn't account explicitly for constraints in the closed-loop motion. Our aim is to extend state-of-the-art task space multi-objectives and multi-sensory whole-body control framework formulated as QP to encompass impact tasks.

Impact dynamics is not well exploited by state-of-the-art practical control strategies. Most impact stabilization papers require *flexible* models with regularization, e.g. the mass-spring-damper [13], [14], [15]. Considered as a transient behavior, impact dynamics is used in stability analysis [16] rather than in explicit control design. This exception is impact models integrated explicitly in an humanoid walking controller based on hybrid zero dynamics, e.g. [17], [18], [19], [20]. Yet these approaches result in a hybrid control scheme that we aim to avoid.

In our recent work [3], we use a task-space force controller [2] to inhibit oscillations and use explicit upper bounds on the impact-induced state jumps to account for hardware limitations, e.g. bounds on impulsive forces and velocity jumps. To the best of our knowledge, our work is the first to embed high-velocity contact-task in the QP formulation that is safe to deal with impacts, while accounting for both hardware limitations and controller feasibility. However, our previous study was achieved for fixed-based robots. When humanoids are to be used, the under-actuated floating-base and balance must be taken into account. Hence, we analytically derive constraints that sustain prior-to-impact unilateral contacts and whole-body balance conditions under impacts that are seamlessly integrated in the continuous dynamic domain multi-objective QP controller [2].

The ZMP is widely used as a balance criterion for biped walking [21], and recently extended to a multi-contact setting in [22]. For trajectory planning tasks that require large impulsive forces, e.g. a nailing task, such as in [4] and a wooden piece breaking task in [5], ZMP is used to analyze the stability of each robot configuration instance. Introducing the impact-robust ZMP constraint into the QP controller allows more reliable and robust motions generation.

III. CONTINUOUS TIME-DOMAIN QP FORMULATION

The detailed QP formulation can be found in [2]. Here we focus on the most pertinent parts we use, i.e. the contact and ZMP constraints in Sec. III-A and Sec. III-B respectively. We then summarize the usual form of the QP controller in Sec. III-C to mathematically highlight why state-of-the-art QP controllers could become infeasible.

A. Contact Constraint

1) *Geometric Constraint:* For each contact of the robot with its surrounding, differentiation of the kinematics model

leads to $J\ddot{\mathbf{q}} + \dot{J}\dot{\mathbf{q}} = 0$, where $J(\mathbf{q})$ is the robot contact Jacobian and \mathbf{q} denotes the generalized coordinate of the robot. We restrict zero relative motion at the contact by:

$$J\ddot{\mathbf{q}} + \dot{J}\dot{\mathbf{q}} = -\frac{\mathbf{v}}{\Delta t}, \quad (1)$$

where \mathbf{v} denotes the actual robot contact-point velocity, and Δt denotes the sampling period.

2) *Center of Pressure Constraint*: Assuming we have a given number of adjacent contact points forming a closed convex contact planar surface \mathcal{S} with a single contact normal n . In view of the local external force \mathbf{f} and moment $\boldsymbol{\tau}$, the center of pressure (CoP) is given as: $\mathbf{p}_x = -\frac{\boldsymbol{\tau}_y}{\mathbf{f}_n}$, $\mathbf{p}_y = \frac{\boldsymbol{\tau}_x}{\mathbf{f}_n}$. x and y are the contact tangent space components, and

$$[\mathbf{p}_x, \mathbf{p}_y] \in \mathcal{S} \quad (2)$$

As long as the contact persists, i.e. $\mathbf{f}_n > 0$, the constraints (2) are always non-singular. We can reformulate the CoP constraint (2) in a matrix form, that is:

$$A_c \mathbf{f} \leq \mathbf{0}. \quad (3)$$

B. Bounded ZMP

If using the zero moment point (ZMP) as the dynamic equilibrium criteria, the ZMP point shall be inside the support polygon having normal n (in co-planar contacts): $\mathbf{z} \in \mathcal{S}$. When $n = [0, 0, 1]^\top$ (opposite to the gravity direction), the ZMP expresses as:

$$z_x = -\frac{\sum \boldsymbol{\tau}_y}{\sum \mathbf{f}_n}, \quad z_y = \frac{\sum \boldsymbol{\tau}_x}{\sum \mathbf{f}_n}. \quad (4)$$

We assume that the support polygon is convex and the half-plane representation $\mathbf{A}_x, \mathbf{A}_y, \mathbf{B} \in \mathbb{R}^{n \times 1}$ is available:

$$[\mathbf{A}_x \quad \mathbf{A}_y] \begin{bmatrix} z_x \\ z_y \end{bmatrix} \leq \mathbf{B}.$$

Substituting z_x, z_y defined by (4), we can obtain the following constraint on the external wrenches $\sum \mathbf{F}$:

$$\underbrace{[\mathbf{A}_y \quad -\mathbf{A}_x \quad \mathbf{0} \quad \mathbf{0} \quad \mathbf{0} \quad -\mathbf{B}]}_{A_z} \sum \mathbf{F} \leq \mathbf{0}. \quad (5)$$

C. QP controller for a humanoid robot

Our QP controller is built from desired task objectives (that shall be met at best in the QP cost function) and gathers desired task constraints (that shall be met strictly, as part of the QP constraints). Thus, in the continuous time-domain, our QP controller for a humanoid robot is enhanced by the previous constraints, in plus of the common usual ones such as joint limits, collision avoidance, torque limits... that we do not mention:

$$\begin{aligned} \min_{\mathbf{x}: (\dot{\mathbf{q}}, \mathbf{f}_\lambda)} \quad & \sum_{i \in \mathcal{I}_o} w_i \|e_i(\mathbf{x})\|^2 \\ \text{s.t.} \quad & \text{Common usual constraints,} \\ & \text{Contact constraints: (1), (3),} \\ & \text{Bounded ZMP: (5),} \end{aligned} \quad (6)$$

where the set \mathcal{I}_o can include any task, e.g. motion tasks, impedance tasks and so on; $e(\mathbf{x})$ denotes the task error

function weighted by w_i . $e(\mathbf{x})$ is linear in terms of the decision variable $\dot{\mathbf{q}}$ and discretized friction cone contact forces \mathbf{f}_λ , see [2] for more details, so are all the constraints of the QP.

Impacts result in instantaneous jumps of the joint velocities $\dot{\mathbf{q}}$, joint torques, and contact forces \mathbf{f} , which are present in the constraints of the QP controller (6). Indeed, such an abrupt jump could result in a not feasible QP for the next control iteration and no command can be issued as exemplified in [3]. For humanoids, it can also result on falls.

IV. PROPOSED QP CONTROLLER

We present the estimation of impulse propagation in Sec. IV-A and IV-B. The latter is used to explicitly derive the influence of the impact on the hardware limits (Sec. IV-C), contact forces (Sec. IV-D), and balance constraints (Sec. IV-E). We integrate impact-aware constraints in our multi-objective whole-body controller in Sec. IV-F.

A. Impact dynamics

Let \vec{n} be the impact surface normal, and c_r the coefficient of restitution (we discuss how these parameters are obtained later in Sec. V-A). Projecting the pre-impact end-effector velocity $\dot{\mathbf{x}}^-$ along \vec{n} , we can predict the post-impact end-effector velocity $\dot{\mathbf{x}}^+$ as

$$\dot{\mathbf{x}}^+ = -c_r P_{\vec{n}} \dot{\mathbf{x}}^- + (I - P_{\vec{n}}) \dot{\mathbf{x}}^-,$$

where $P_{\vec{n}} = \vec{n} \vec{n}^\top$. The end-effector velocity jump is defined as:

$$\Delta \dot{\mathbf{x}} = \dot{\mathbf{x}}^+ - \dot{\mathbf{x}}^- = \underbrace{-(1 + c_r) P_{\vec{n}}}_{P_\Delta} \dot{\mathbf{x}}^-.$$

Thus at time step k , we predict the end-effector velocity jump $\Delta \dot{\mathbf{x}}_{k+1}$ as:

$$\Delta \dot{\mathbf{x}}_{k+1} = P_\Delta \dot{\mathbf{x}}_{k+1}^-, \quad (7)$$

where $\dot{\mathbf{x}}_{k+1}^- = \mathbf{J}_{\dot{\mathbf{x}}^-} \dot{\mathbf{q}}_{k+1}$, $\mathbf{J}_{\dot{\mathbf{x}}^-} = \mathbf{J}_{k+1} = \mathbf{J}_k + \dot{\mathbf{J}}_k \Delta t$ and $\dot{\mathbf{q}}_{k+1} = \dot{\mathbf{q}}_k + \ddot{\mathbf{q}}_k \Delta t$. The $\dot{\mathbf{q}}_k$ is obtained from the robot current state and Δt denotes the sampling period. We re-write (7) as a function of the optimization variable $\ddot{\mathbf{q}}_k$:

$$\Delta \dot{\mathbf{x}}_{k+1} = P_\Delta (\mathbf{J}_k \Delta t \ddot{\mathbf{q}}_k + \dot{\mathbf{J}}_k \Delta t^2 \ddot{\mathbf{q}}_k + \mathbf{J}_k \dot{\mathbf{q}}_k + \dot{\mathbf{J}}_k \dot{\mathbf{q}}_k \Delta t), \quad (8)$$

where we can neglect the term $\dot{\mathbf{J}}_k \Delta t^2 \ddot{\mathbf{q}}_k \approx 0$ as $\Delta t \leq 5$ ms.

B. Impulse prediction

Let us consider a humanoid robot with n DoF and m end-effectors with established contacts. The impact is about to happen at another end-effector $m+1$ (e.g. $m = 2$ in the case where two feet are in contact with the ground, one gripper is free and the other is about to achieve a desired impact with the wall). We not only need to predict the impulse I_{m+1} but also how it propagates along the kinematic tree to any of the previously defined m task effectors. Namely, in addition to I_{m+1} , we need to predict the propagated impulses I_i for $i = 1 \dots m$ and the impact-induced joint velocity jumps of all the kinematic branches $\Delta \dot{\mathbf{q}} = \dot{\mathbf{q}}^+ - \dot{\mathbf{q}}^-$.

Let $\mathbf{x} = [\mathbf{x}_1^\top, \dots, \mathbf{x}_{m+1}^\top]^\top \in \mathbb{R}^{3(m+1)}$ the end-effectors coordinates and associated Jacobians $\mathbf{J} =$

$[J_1^\top, \dots, J_{m+1}^\top]^\top \in \mathbb{R}^{3(m+1) \times n}$, we use the operational space dynamics (or equivalently the *articulated-body inertia* presented in Sec. 7.1 of the book by Featherstone [9]) to characterize the impulse propagation between I_{m+1} and I_i for $i = 1, \dots, m$:

$$\ddot{\mathbf{x}} = \Lambda(\mathbf{q})^{-1} \mathbf{f} + \boldsymbol{\beta} \quad (9)$$

where $\mathbf{f} \in \mathbb{R}^{3(m+1)}$ denotes all the external contact forces and the impulsive force, the inverse operational space inertial matrix $\Lambda(\mathbf{q})^{-1} \in \mathbb{R}^{3(m+1) \times 3(m+1)}$ is defined as: $\Lambda(\mathbf{q})^{-1} = JM^{-1}J^\top$. The remaining acceleration bias $\boldsymbol{\beta}$ that we do not use, are defined in [23]. We can compute a first-order approximation of predicted $\Lambda(\mathbf{q}_{k+1})^{-1}$ as follows:

$$(J_k + \Delta t \dot{J}_k)(M_k + \Delta t \dot{M}_k)^{-1}(J_k^\top + \Delta t \dot{J}_k^\top) \quad (10)$$

where $\dot{M}_k = C_k + C_k^\top$ computation is readily available in the QP control framework. Integrating the equations of motion (9) over the impact duration δt and expanding the inverse operational space inertia matrix Λ^{-1} , we can obtain

$$\begin{bmatrix} \Delta \dot{\mathbf{x}}_1 \\ \Delta \dot{\mathbf{x}}_2 \\ \vdots \\ \Delta \dot{\mathbf{x}}_{m+1} \end{bmatrix} = \begin{bmatrix} \Lambda_{11}^{-1} & \cdots & \Lambda_{1(m+1)}^{-1} \\ \Lambda_{21}^{-1} & \cdots & \Lambda_{2(m+1)}^{-1} \\ \vdots & \ddots & \vdots \\ \Lambda_{(m+1)1}^{-1} & \cdots & \Lambda_{(m+1)(m+1)}^{-1} \end{bmatrix} \begin{bmatrix} I_1 \\ I_2 \\ \vdots \\ I_{m+1} \end{bmatrix}$$

where the inverse inertial matrix Λ_{ij}^{-1} relates the external impulse $I_j = \int \mathbf{f}_j \delta t$, acting on the j -th end-effector to the i -th end-effector velocity jump $\delta \dot{\mathbf{x}}_i$. In a compact form we have:

$$\Delta \dot{\mathbf{x}} = \Lambda^{-1} I \quad (11)$$

We can re-write each $\Delta \dot{\mathbf{x}}_i$ using the kinematics

$$\Delta \dot{\mathbf{x}}_i = J_i \Delta \dot{\mathbf{q}} \quad \text{for } i = 1 \dots m+1, \quad (12)$$

which simplifies (11) to:

$$J \Delta \dot{\mathbf{q}} = \Lambda^{-1} I. \quad (13)$$

Knowing the end-effector velocity jump $\Delta \dot{\mathbf{x}}_{m+1}$ from (8), we can predict $\Delta \dot{\mathbf{q}}$, the impulse I_{m+1} and the propagated impulses of the end-effectors with established contact I_i for $i = 1, \dots, m$, using an auxiliary QP with the optimization variables $\mathbf{u} = [\Delta \dot{\mathbf{q}}, I_1, \dots, I_{m+1}]^\top$:

$$\begin{aligned} \min_{\mathbf{u}} \quad & \frac{1}{2} \mathbf{u}^\top \mathbf{u} \\ \text{s.t.} \quad & \text{Impulse propagation: (13)} \\ & \text{Initial condition: } J_{m+1} \Delta \dot{\mathbf{q}} = \Delta \dot{\mathbf{x}}_{m+1} \end{aligned} \quad (14)$$

Since (14) is an equality-constrained QP, its analytical solution is available. Re-writing (14) in the standard form:

$$\begin{aligned} \min_{\mathbf{u}} \quad & \frac{1}{2} \mathbf{u}^\top \mathbf{u} \\ \text{s.t.} \quad & [J, \quad -\Lambda^{-1}] \mathbf{u} = 0, \\ & [J_{m+1}, \quad 0] \mathbf{u} = \Delta \dot{\mathbf{x}}_{m+1} \end{aligned} \quad (15)$$

The *KKT system* associated with (15) is:

$$\underbrace{\begin{bmatrix} I & A^\top \\ A & 0 \end{bmatrix}}_K \begin{bmatrix} \mathbf{u} \\ \boldsymbol{\lambda} \end{bmatrix} = \begin{bmatrix} 0 \\ \mathbf{b} \end{bmatrix},$$

where $\boldsymbol{\lambda}$ denotes the associated Lagrange multipliers, $\mathbf{b} = [0, \dots, \Delta \dot{\mathbf{x}}_{m+1}^\top]^\top$ and $A = \begin{bmatrix} J, & -\Lambda^{-1} \\ J_{m+1}, & 0 \end{bmatrix}$.

As $\mathbf{b} \in \mathbb{R}^{3(m+1)}$ has all zeros except the last three elements, which is the predicted $\Delta \dot{\mathbf{x}}_{m+1}$ given by (8), we can predict the following for $i = 1, \dots, m+1$ at time t_{k+1} :

$$\Delta \dot{\mathbf{q}}^* = K_{\Delta \dot{\mathbf{q}}}^{-1} \Delta \dot{\mathbf{x}}_{m+1}, I_i^* = K_i^{-1} \Delta \dot{\mathbf{x}}_{m+1}, \quad (16)$$

where $K_{\Delta \dot{\mathbf{q}}}^{-1} \in \mathbb{R}^{n \times 3}$ and $K_i^{-1} \in \mathbb{R}^{3 \times 3}$ are taken accordingly from the last three columns of the inverse K^{-1} .

The predictions defined in (16) are functions of $\ddot{\mathbf{q}}$ due to the predicted $\delta \dot{\mathbf{x}}_{m+1}$ (8). Thus we can use (16) to formulate impact-aware constraints for a QP controller, e.g. (6), to generate feasible motion in view of the hardware limits, existing unilateral contacts and ZMP conditions.

Remark IV.1. *The least norm problem (15) has a unique optimal solution $\mathbf{u}^* = K^{-1} \mathbf{b}$ as long as matrix A has full row rank and I is positive definite [24]. In view of the components of matrix A , as long as the robot is not in a singular configuration, the conditions are fulfilled.*

If there is more than one impact, we can and add it to the auxiliary QP(14) as an additional constraint

$$J_{m+2} \delta \dot{\mathbf{q}} = \delta \dot{\mathbf{x}}_{m+2}.$$

C. Hardware limit constraints

We formulate the constraints (17) and (18) to prevent violating the hardware limits, i.e. the limited joint velocities $[\underline{\dot{\mathbf{q}}}, \bar{\dot{\mathbf{q}}}]$ and the limited impulsive joint torques $[\underline{\boldsymbol{\tau}}, \bar{\boldsymbol{\tau}}]$.

1) *Joint velocity limit:* As analyzed by [3], we can restrict the post-impact joint velocity $\dot{\mathbf{q}}^+ \in [\underline{\dot{\mathbf{q}}}, \bar{\dot{\mathbf{q}}}]$ by:

$$\begin{aligned} \Delta \dot{\mathbf{q}}(t_{k+1}) &\leq \dot{\mathbf{q}} - \dot{\mathbf{q}}(t_k) \\ -\Delta \dot{\mathbf{q}}(t_{k+1}) &\leq -(\dot{\mathbf{q}} - \dot{\mathbf{q}}(t_k)) \end{aligned}$$

We can reformulate the above to restrict $\ddot{\mathbf{q}}$:

$$\begin{aligned} \mathcal{J}_{\Delta \dot{\mathbf{q}}} \ddot{\mathbf{q}} \Delta t &\leq \dot{\mathbf{q}} - \dot{\mathbf{q}} - \mathcal{J}_{\Delta \dot{\mathbf{q}}} \dot{\mathbf{q}} \\ -\mathcal{J}_{\Delta \dot{\mathbf{q}}} \ddot{\mathbf{q}} \Delta t &\leq -(\dot{\mathbf{q}} - \dot{\mathbf{q}} - \mathcal{J}_{\Delta \dot{\mathbf{q}}} \dot{\mathbf{q}}) \end{aligned} \quad (17)$$

where $\mathcal{J}_{\Delta \dot{\mathbf{q}}}$ is defined in view of the predicted $\Delta \dot{\mathbf{x}}_{m+1}$ (8) and $\Delta \dot{\mathbf{q}}$ (16):

$$\Delta \dot{\mathbf{q}}(t_{k+1}) = \underbrace{K_{\Delta \dot{\mathbf{q}}}^{-1} P_{\Delta} J_{m+1}}_{\mathcal{J}_{\Delta \dot{\mathbf{q}}}} (\dot{\mathbf{q}}(t_k) + \ddot{\mathbf{q}}(t_k) \Delta t).$$

2) *Impulsive joint torque:* Following previous examples, e.g. [5], we define the impulsive end-effector forces:

$$\bar{\mathbf{f}}_i = \frac{I_i}{\delta t} \quad \text{for } i = 1, \dots, m+1.$$

We can predict the whole-body impulsive joint torque:

$$\Delta \boldsymbol{\tau} = \sum_{i=1}^{m+1} \boldsymbol{\tau}_i = \sum_{i=1}^{m+1} J_i^\top \bar{\mathbf{f}}_i = \frac{1}{\delta t} \left(\sum_{i=1}^{m+1} J_i^\top K_i^{-1} \right) \Delta \dot{\mathbf{x}}_{m+1},$$

and restrict it by:

$$\begin{aligned} \frac{\Delta t}{\delta t} \mathcal{J}_{\Delta\tau} \ddot{\mathbf{q}} &\leq \Delta\bar{\boldsymbol{\tau}} - \frac{1}{\delta t} \mathcal{J}_{\Delta\tau} \dot{\mathbf{q}} \\ -\frac{\Delta t}{\delta t} \mathcal{J}_{\Delta\tau} \ddot{\mathbf{q}} &\leq -(\Delta\boldsymbol{\tau} - \frac{1}{\delta t} \mathcal{J}_{\Delta\tau} \dot{\mathbf{q}}), \end{aligned} \quad (18)$$

where $\mathcal{J}_{\Delta\tau}$ is defined using the predicted $\Delta\dot{\mathbf{x}}_{m+1}$ and $\Delta\boldsymbol{\tau}$:

$$\Delta\boldsymbol{\tau}(t_{k+1}) = \frac{1}{\delta t} \underbrace{\left(\sum_{i=1}^{m+1} J_i^\top K_i^{-1} \right) P_{\Delta} J_{m+1}}_{\mathcal{J}_{\Delta\tau}} (\dot{\mathbf{q}}(t_k) + \ddot{\mathbf{q}}(t_k) \Delta t).$$

D. Holding Established Contacts

We propose the constraint (19) and (20) to sustain an established contact by restricting the center of pressure and fulfilling the friction cone.

1) *Center of pressure constraint:* Due to the propagated impulse, the constraint (3) becomes

$$A_c(\bar{\mathbf{F}} + \mathbf{F}) \leq 0 \Rightarrow A_c \bar{\mathbf{F}} \leq -A_c \mathbf{F},$$

where \mathbf{F} denotes the measured wrench of an established contact and $\bar{\mathbf{F}} = [\mathbf{0}^\top, \bar{\mathbf{f}}^\top]^\top$. Let A_{c2} as the columns of A_c corresponding to force, we have:

$$A_{c2} \bar{\mathbf{f}} \leq -A_c \mathbf{F}.$$

We can re-write the above to restrict $\ddot{\mathbf{q}}$:

$$A_{c2} \mathcal{J}_f \ddot{\mathbf{q}} \frac{\Delta t}{\delta t} \leq -A_c \mathbf{F} - A_{c2} \mathcal{J}_f \dot{\mathbf{q}} \frac{1}{\delta t}, \quad (19)$$

where we defined the Jacobian \mathcal{J}_f in view of the impulsive force and the predicted impulse I^* (16):

$$\bar{\mathbf{f}} = \frac{I^*}{\delta t} = \frac{1}{\delta t} \underbrace{K_i^{-1} P_{\Delta} J_{m+1}}_{\mathcal{J}_f} (\dot{\mathbf{q}}(t_k) + \ddot{\mathbf{q}}(t_k) \Delta t).$$

2) *Fulfilling friction cone:* We prevent slippage by limiting the predicted contact force within the friction cone:

$$N_{\bar{\mathbf{n}}}(\mathbf{f} + \bar{\mathbf{f}}) \leq \mu P_{\bar{\mathbf{n}}}(\mathbf{f} + \bar{\mathbf{f}}).$$

If we define $P_{\mu} = I - \bar{\mathbf{n}}\bar{\mathbf{n}}^\top - \mu \bar{\mathbf{n}}\bar{\mathbf{n}}^\top$, we can re-write the constraint as $P_{\mu} \bar{\mathbf{f}} \leq -P_{\mu} \mathbf{f}$ or equivalently:

$$P_{\mu} \mathcal{J}_f \ddot{\mathbf{q}} \frac{\Delta t}{\delta t} \leq -P_{\mu}(\mathbf{f} + \mathcal{J}_f \dot{\mathbf{q}} \frac{1}{\delta t}). \quad (20)$$

E. Bounded ZMP

Given the impulsive forces of all the end-effectors either with an established contact or undergoing an impact, we can predict the impact-induced jump of the ZMP to fulfill the ZMP constraint (5):

$$A_Z \left(\sum_{i=1}^{m+1} \mathbf{F} + \sum_{i=1}^{m+1} \bar{\mathbf{F}} \right) \leq 0 \Rightarrow A_Z \sum_{i=1}^{m+1} A_i \bar{\mathbf{f}}_i \leq - \sum_{i=1}^{m+1} A_Z \mathbf{F}_i,$$

where A_i denotes the transformation matrix that calculates the equivalent wrench in the inertial frame due to the impulsive force $\bar{\mathbf{f}}_i$, the wrench \mathbf{F} denotes the sum of the external wrenches in the inertial frame. Thus we can restrict the robot joint accelerations $\ddot{\mathbf{q}}$ with the following inequality:

$$A_Z \sum_{i=1}^{m+1} (A_i \mathcal{J}_{f_i}) \ddot{\mathbf{q}} \frac{\Delta t}{\delta t} \leq -A_Z \left(\sum_{i=1}^{m+1} \mathbf{F}_i + \frac{1}{\delta t} \sum_{i=1}^{m+1} (A_i \mathcal{J}_{f_i}) \dot{\mathbf{q}} \right). \quad (21)$$

F. Impact-robust QP controller synthesis

Should there exists an incoming impact at one end-effector, we need to solve the modified QP:

$$\begin{aligned} \min_{\mathbf{x}: (\ddot{\mathbf{q}}, \mathbf{f}_\lambda)} \quad & \sum_{i \in \mathcal{I}_o} w_i \|e_i(\mathbf{x})\|^2 \\ \text{s.t.} \quad & \text{Common usual constraints,} \\ & \text{Hardware constraints: (17)(18),} \\ & \text{Holding contact constraints: (19), (20),} \\ & \text{ZMP constraint: (21).} \end{aligned} \quad (22)$$

Compared to the usual QP controller (6), a humanoid robot controlled by (22) is always able to guarantee the hardware limits, maintain the established contacts and the ZMP condition while fulfilling the task objectives included in \mathcal{I}_o . Thus we do not need to make any assumption on the impact timing or manually choose a safe yet near-zero contact velocity, rather, (22) would generate the maximal contact velocities with respect to the feasibility of the constraints (17-21).

V. EXPERIMENT

We use a full-size humanoid robot HRP-4 to validate that the proposed QP controller is able to generate feasible contact velocities with respect to the constraints (17-21). Using the experimental parameters summarized in Sec. V-A, we present the experimental results in Sec. V-B where the robot generated the maximal contact velocity along the direction of interest rather than planning the contact at a specific location, i.e. being aware of the contact surface location. In the snapshots shown in Fig 1, the robot hit the wall with a contact velocity of 0.35 m/s and then regulate the contact force to 15 N. We encourage interested readers to check the experiment videos.

A. Parameters

In order to exert the impulse, We mounted a 3D printed plastic palm of 3 cm thickness. The robot keeps the maximal available contact velocity until the force sensor mounted on the wrist reached the impact detection threshold, i.e. 20 N. In order to correctly observe the post-impact state jumps, we choose not to use a stabilizer. For the established contacts, we choose the friction coefficient as 0.7.

Based on several trial runs, we choose the coefficient of restitution $c_r = 0.02$, which indicates trivial rebound. It leads to a reasonable prediction of the impulsive force, see Fig. 4.

The QP controller runs at 200 Hz, which gives the sampling period $\Delta t = 5$ ms. The impact duration δt appears in the constraints (18-21), where the predicted impulsive forces are used. As the ATI-45 force-torque sensors are read at 200 Hz, we choose the same period for the impact duration: $\delta t = 5$ ms.

B. Constraints validation

The proposed QP controller (22) autonomously determines the *feasible* contact velocity. Thus we assign an exceptionally high contact velocity, i.e. 0.8 m/s , to check if the hardware limits and the standing stability are satisfied. The ZMP profiles generated with different constraints settings reveal that the support polygon \mathcal{S} , which is the enclosing convex polygon of the feet contact areas, is too conservative. More applicable stability measures or an extended support polygon are needed to exploit the maximal contact velocity.

In order to fulfill the impulsive joint torque bounds, see Fig. 3, the QP controller (22) updates the *feasible* contact velocity set-point in real-time as shown in Fig. 2. In all the plots, we use a dashed black line to indicate the impact time.

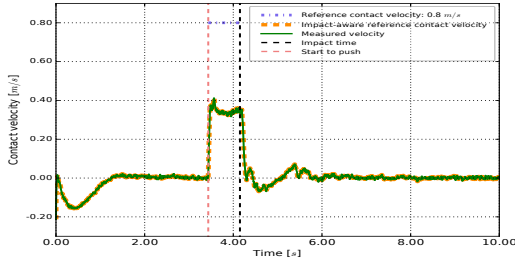


Fig. 2: Given the reference 0.8 m/s , the QP controller (22) autonomously determined the safe contact velocity.

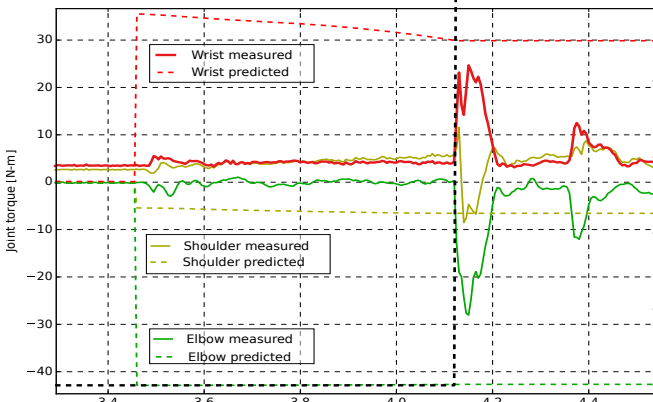


Fig. 3: Considering three joints taken from the shoulder, elbow, and wrist, at the impact time the joint torque calculated by $J^T \mathbf{f}$, where \mathbf{f} is read from the sensor, is close to the prediction $\Delta \tau$ and smaller than the corresponding bounds of $\pm 46 \text{ N} \cdot \text{m}$, $\pm 42.85 \text{ N} \cdot \text{m}$ and $\pm 85.65 \text{ N} \cdot \text{m}$.

The predicted impulsive force is shown in Fig. 4. After the impact is detected, the contact velocity did not reduce to zero as the robot started an admittance controller to regulate the *post-impact* contact force to 15 N , which is shown between 10s and 15s of Fig. 4.

From the snapshots in Fig. 1, the robot did not fall. However if we check the ZMP (along the normal direction of the wall surface) plotted in Fig. 5, we can find that the ZMP temporarily jumped outside the bound (see the 2D view in Fig. 6a).

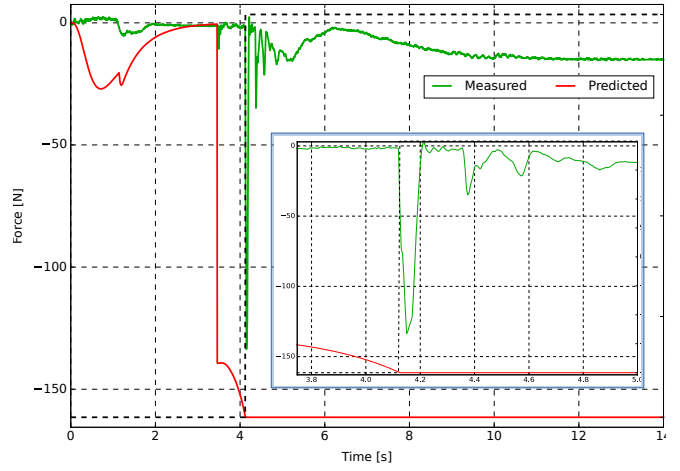


Fig. 4: The impact detected at 4.18 s generated impulsive force 133 N which is smaller the predicted impulsive force 161 N . The conservative prediction leads to safe motion generation in view of the worst-case impact.

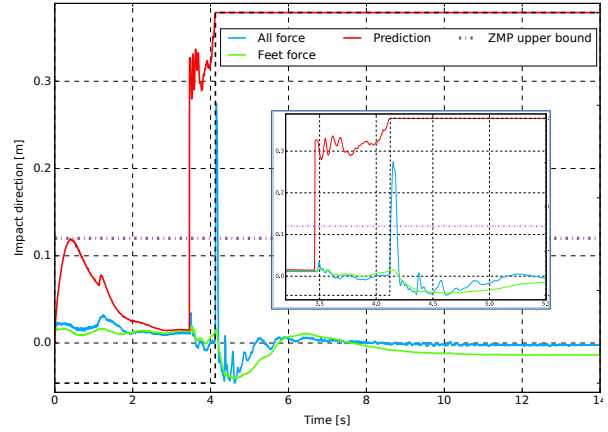
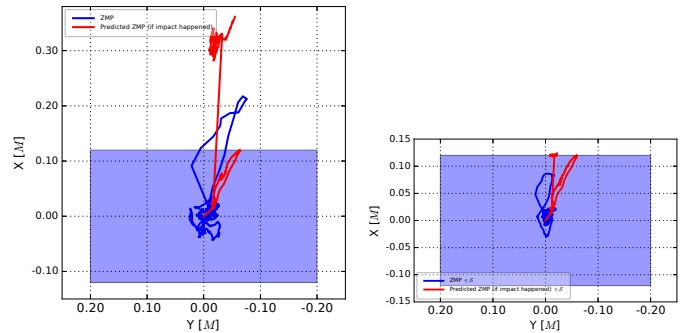


Fig. 5: Comparison of ZMP (along the impact direction) computed with feet force (light green), both feet and measured impulsive force at the wrist (light blue), and both feet and predicted impulsive force at the wrist (red).



(a) Contact velocity 0.35 m/s . (b) Contact velocity 0.11 m/s .

Fig. 6: In fig. 6a we can predict the ZMP would jump outside the support polygon \mathcal{S} due to the contact velocity 0.35 m/s . In fig. 6b the contact velocity is reduced to 0.11 m/s , the ZMP is strictly bounded within the support polygon \mathcal{S} .

Using the predicted impulsive force shown in Fig. 4, we

can actually predict the ZMP jump. In Fig. 5, we can see that the predicted ZMP in case of impact (red curve) is well above the actual jump. Thus using this information we can keep the ZMP strictly bounded. In Fig. 7 and the 2D view Fig. 6b, we plot the ZMP of another experiment where the only difference is that the wrench generated by the predicted impulsive force of the hand is included in the constraint (21). Compared to Fig. 5 and Fig. 6a, both the predicted ZMP under impact and the actual ZMP are well bounded by the support polygon. Not surprisingly, the price we paid for being more stable is slowing down the contact velocity to 0.11 m/s .

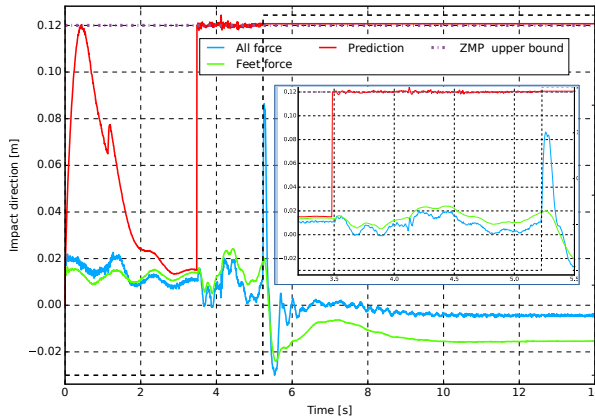


Fig. 7: Using predicted impulsive force at the wrist in constraint (21), we can strictly bound the ZMP $z \in \mathcal{S}$.

VI. CONCLUSION

Impact-induced state jumps, i.e. joint velocity and impulsive forces, challenge the hardware limits of a robot. In the case of a humanoid, the problem gets even more complicated due to its complicated kinematic structure and additional requirements for contact and balance maintenance. Through analysis of the impact-induced state jumps propagation between different kinematic branches, we propose a set of modified constraints to guarantee the feasibility of the robot configuration such that the QP controller can exploit the maximal contact velocity of a humanoid robot. Through experiments performed by an HRP-4 robot, we achieved contact velocity at 0.35 m/s and maximal impulsive force 133 N , which are significant compared to the motion generated by the conventional impedance control law. To the best of our knowledge, we are the first to propose an impact-aware humanoid robot motion generation controller based on quadratic optimization.

In the future, we need a less conservative stability condition rather than restricting ZMP strictly inside the support polygon: $z \in \mathcal{S}$, whose conservativeness has been already revealed from the experiments.

REFERENCES

- [1] Y.-F. Zheng and H. Hemami, "Mathematical modeling of a robot collision with its environment," *Journal of Field Robotics*, vol. 2, no. 3, pp. 289–307, 1985.
- [2] K. Bouyarmane, K. Chappellet, J. Vaillant, and A. Kheddar, "Quadratic programming for multirobot and task-space force control," *IEEE Transactions on Robotics*, vol. 35, no. 1, pp. 64–77, February 2019.
- [3] Y. Wang and A. Kheddar, "Impact-friendly robust control design with task-space quadratic optimization," in *Proceedings of Robotics: Science and Systems*, Freiburg, Germany, 24–26 June 2019.
- [4] T. Tsujita, A. Konno, S. Komizunai, Y. Nomura, T. Owa, T. Myojin, Y. Ayaz, and M. Uchiyama, "Analysis of nailing task motion for a humanoid robot," in *IEEE/RSJ International Conference on Intelligent Robots and Systems*, 22–26 September 2008, pp. 1570–1575.
- [5] A. Konno, T. Myojin, T. Matsumoto, T. Tsujita, and M. Uchiyama, "An impact dynamics model and sequential optimization to generate impact motions for a humanoid robot," *The International Journal of Robotics Research*, vol. 30, no. 13, pp. 1596–1608, 2011.
- [6] S. Pashah, M. Massenzio, and E. Jacquelin, "Prediction of structural response for low velocity impact," *International Journal of Impact Engineering*, vol. 35, no. 2, pp. 119–132, 2008.
- [7] S. Haddadin, A. Albu-Schäffer, and G. Hirzinger, "Requirements for safe robots: Measurements, analysis and new insights," *The International Journal of Robotics Research*, vol. 28, no. 11–12, pp. 1507–1527, 2009.
- [8] D. E. Stewart, "Rigid-body dynamics with friction and impact," *SIAM review*, vol. 42, no. 1, pp. 3–39, 2000.
- [9] R. Featherstone, *Rigid body dynamics algorithms*. Springer, 2014.
- [10] Y.-B. Jia, M. Gardner, and X. Mu, "Batting an in-flight object to the target," *The International Journal of Robotics Research*, vol. 38, no. 4, pp. 451–485, 2019.
- [11] Y.-B. Jia and F. Wang, "Analysis and computation of two body impact in three dimensions," *Journal of Computational and Nonlinear Dynamics*, vol. 12, no. 4, p. 041012, 2017.
- [12] M. Rijnen, E. de Mooij, S. Traversaro, F. Nori, N. van de Wouw, A. Saccon, and H. Nijmeijer, "Control of humanoid robot motions with impacts: Numerical experiments with reference spreading control," in *IEEE International Conference on Robotics and Automation*, 2017, pp. 4102–4107.
- [13] G. Hu, C. Makkar, and W. E. Dixon, "Energy-based nonlinear control of underactuated euler-lagrange systems subject to impacts," *IEEE Transactions on Automatic Control*, vol. 52, no. 9, pp. 1742–1748, 2007.
- [14] R. Z. Stanisic and Á. V. Fernández, "Adjusting the parameters of the mechanical impedance for velocity, impact and force control," *Robotica*, vol. 30, no. 4, pp. 583–597, 2012.
- [15] D. Heck, A. Saccon, N. Van de Wouw, and H. Nijmeijer, "Guaranteeing stable tracking of hybrid position-force trajectories for a robot manipulator interacting with a stiff environment," *Automatica*, vol. 63, pp. 235–247, 2016.
- [16] P. R. Pagilla and B. Yu, "A stable transition controller for constrained robots," *IEEE/ASME transactions on mechatronics*, vol. 6, no. 1, pp. 65–74, 2001.
- [17] Y. Hurmuzlu, F. Génot, and B. Brogliato, "Modeling, stability and control of biped robots—a general framework," *Automatica*, vol. 40, no. 10, pp. 1647–1664, 2004.
- [18] P. van Zutven, D. Kostić, and H. Nijmeijer, "On the stability of bipedal walking," in *Simulation, Modeling, and Programming for Autonomous Robots*, N. Ando, S. Balakirsky, T. Hemker, M. Reggiani, and O. von Stryk, Eds. Springer Berlin Heidelberg, 2010, pp. 521–532.
- [19] J. W. Grizzle, C. Chevallereau, A. D. Ames, and R. W. Sinnet, "3d bipedal robotic walking: Models, feedback control, and open problems," *IFAC Proceedings Volumes*, vol. 43, no. 14, pp. 505–532, 2010, 8th IFAC Symposium on Nonlinear Control Systems.
- [20] A. Hereid, C. M. Hubicki, E. A. Cousineau, and A. D. Ames, "Dynamic humanoid locomotion: A scalable formulation for HZD gait optimization," *IEEE Transactions on Robotics*, vol. 34, no. 2, pp. 370–387, Apr. 2018.
- [21] S. Kajita, H. Hirukawa, K. Harada, and K. Yokoi, *Introduction to humanoid robotics*. Springer, 2014, vol. 101.
- [22] S. Caron, Q.-C. Pham, and Y. Nakamura, "Zmp support areas for multi-contact mobility under frictional constraints," *IEEE Transactions on Robotics*, vol. 33, no. 1, pp. 67–80, Feb. 2017.
- [23] R. Featherstone, "Exploiting sparsity in operational-space dynamics," *The International Journal of Robotics Research*, vol. 29, no. 10, pp. 1353–1368, 2010.
- [24] S. Boyd and L. Vandenberghe, *Convex optimization*. Cambridge university press, 2004.